JOURNAL OF GUIDANCE, CONTROL, AND DYNAMICS
Vol. 33, No. 4, July–August 2010

Dynamics of Variable-Length Tethered Formations near Libration Points

Jun Zhao,* Zhiqin Cai,† and Zhaohui Qi‡
Dalian University of Technology, Dalian, People's Republic of China

DOI: 10.2514/1.47138

The dynamics of multitethered satellite formations near libration points are presented. The system consists of a parent satellite and subsatellites, connected together in a hub–spoke configuration via variable-length tethers. Based on Hill's approximation, a new dynamical formulation for nonrotating or rotating tethered formations is developed. The equilibrium positions are determined, and linearized analysis is performed for the nonrotating system with constant-length tethers. Numerical simulations using the full nonlinear and time-varying motion equations are carried out for the stationkeeping and reconfiguration stages. For nonrotating systems, the motion of the parent satellite is less stable for larger initial equilibrium positions during stationkeeping, and the tether librations during deployment are more stable than those during retrieval. For rotating systems, the orbital amplitude, orbital direction, and mass ratio have some impact on the stability of the system, and the retrieval is more conducive to keeping the system in its planar configuration when compared with the deployment.

Nomenclature

E_g	=	potential energy term of the formation system
F_{xi}, F_{yi} F_{zi}	=	ith tether influence terms acting on the parent satellite
i	=	number of the subsatellite
L_{di}	=	length of ith tether, m
l_{di}	=	nondimensional length of ith tether
ℓ, τ	=	scales of length and time in Hill's restricted three-body problem
$l_{0,di}$	=	initial nondimensional length of ith tether
m	=	total mass of the formation system, kg
m_P, m_i	=	mass of the parent satellite and ith subsatellite, kg
N	=	total number of the subsatellites
n	=	angular speed of the rotating frame attached to S_E, rad/s
q	=	generalized coordinate
Q_q^F	=	generalized force corresponding to q, N
$\mathbf{R}_P$	=	position vector of the parent satellite relative to Earth
$\mathbf{r}_i$	=	position vector of the ith subsatellite relative to the parent satellite
r_P	=	dimensionless form of the magnitude of the position vector of the parent satellite
S_E	=	body-centered rotating coordinates with the origin at the Earth
S_L	=	additional set of coordinates with the origin at L_2
S_P	=	additional set of coordinates with the origin at the parent satellite
T_f	=	kinetic energy term of the formation system
$\mathbf{v}_P$, $\mathbf{v}_i$	=	velocity vectors of the parent satellite and the ith subsatellite in S_E
x_e, y_e, z_e	=	equilibrium positions of the parent satellite
δx, δy, δz	=	small deviations from equilibrium positions
$\delta\theta_i$, $\delta\phi_i$	=	small deviations from equilibrium angles
ε	=	nondimensional distance of L_2 relative to the Earth in S_E
θ_i, ϕ_i	=	in-plane and out-of-plane rotation angles of the ith tether, deg
θ_{ie}, ϕ_{ie}	=	equilibrium angles of tethers
λ_C, λ_e	=	the coefficient of variable-length tethers
μ_e	=	gravitational parameter of the Earth
μ_i	=	mass ratio of the ith subsatellite
$\boldsymbol{\omega}$	=	angular velocity vector of the rotating frame attached to S_E

I. Introduction

THE libration points, called equilibrium or Lagrangian points, are points where the gravitational and dynamical forces acting on the third body cancel each other out. As is well known, the circularly restricted three-body problem (CRTBP) has five libration points: three collinear and two triangular. Collinear libration points offer unique opportunities for space missions and planetary science. It is expected that sun–Earth collinear libration points will be the locations of choice for a number of large astronomical observatories over the next two decades [1]. Recent work has shown that formation flight with a rigid shape is possible using libration point orbits. However, formation flight in the vicinity of libration points is challenging, with its own unique problems of stability, such as formation reconfiguration, high power consumption to maintain the satellites' relative positions, the inherent instability of dynamics near the collinear libration points, and many other associated issues. To alleviate these concerns, several propellant-free or near propellant-free propulsion techniques have been proposed, including solar sails and spin-stabilized tether systems [2]. The idea of using space tethers has received a great deal of attention in recent years with some existing research on concepts and applications [3–7], but almost all of it deals with single-tethered systems (classical dumbbell model) in low-Earth orbit (LEO). Any generic distribution of more than two masses connected by tethers in a stable configuration is defined as a multitethered formation (constellation) [8]. Tethered formations are divided into two basic categories [9]: static and dynamic. Static formations are formations that do not rotate relative to the orbiting reference frame. Dynamic formations, on the other hand, are formations that do rotate with respect to the orbiting reference frame.

Received 11 September 2009; revision received 12 April 2010; accepted for publication 14 April 2010.

*Ph.D. Candidate, Department of Engineering Mechanics, State Key Laboratory of Structural Analysis for Industrial Equipment; ppwzj1981@gmail.com.

†Associate Professor, Department of Engineering Mechanics, State Key Laboratory of Structural Analysis for Industrial Equipment; zhqcai@dlut.edu.cn.

‡Professor, Department of Engineering Mechanics, State Key Laboratory of Structural Analysis for Industrial Equipment; zhaohuiq@dlut.edu.cn.

Probably, the potential range of applications for a multitethered formation is the greatest in space interferometry for both LEO and deep space. An example of this type of application in deep space has been proposed for the Submillimeter Probe of the Evolution of Cosmic Structure (SPECS) mission [10–13]. The advantage of using tethers is that a variable and controllable baseline can be achieved by deploying or retracting tethers, with a much smaller fuel consumption for reconfiguring the spacecraft, as compared with the case of untethered formation, in which onboard thrusting is continuously required.

There have been some investigations of the dynamics and control of tethered dynamic formations in LEO over the years [14–18]. For almost all of these studies, it is assumed that attitude dynamics do not affect the orbital dynamics, and the masses of the subsatellites are much smaller than the mass of the parent satellite. Comparatively few studies have been presented on the coupling between attitude dynamics and orbital dynamics. Additionally, unlike LEO, the libration point orbits are inherently unstable, and small perturbations can make the system depart from the predefined orbit. Hence, in order to study the coupling between tether librations and the orbital motion of tethered satellite formations near libration points, a new mathematical model should be developed.

Studies have been carried out on the dynamics of multitethered formations near libration points. Gates [19] derived the equations of motion and the tether tension equations for an arbitrarily configured multitethered system near libration points in the CRTBP, without explicitly considering gravitational forces acting on the system. The rotation of the sun–Earth frame was also not considered in the analysis. However, the effect of higher-order terms of the mutual gravity field and frame rotation may play an important role in the dynamics and stability of the tethered satellite near a libration point. Farquhar [20], and then Misra et al. [21], studied the dynamics of the classical dumbbell model near libration points, using different methods in which the mutual gravity field was considered to be based on the CRTBP, and the system center of mass was assumed to be held at the libration points. It was shown that the system center of mass became stable if an appropriate variation of the tether length was accomplished. Suggestions for further studies were given by Farquhar [20]: namely, the stabilization of tethered satellites in a large halo orbit and numerical studies using the full nonlinear and time-varying equations of motion. Most recently, Peláez, et al. [22] substantially extended the reach of previous works by analyzing, in a systematic way, inert and electrodynamic tethers and focusing on both the collinear and the triangular libration points of the CRTBP. Both the classical dumbbell model and extended dumbbell model were considered in their research. Some interesting results based on the Hill approximation were presented. Wong and Misra [23] performed a preliminary study of a multitethered system in the CRTBP, where the system was arranged in a hub-and-spoke (HAS) configuration with fixed tether lengths, and the free dynamics were studied under the prescription that the motion of the parent satellite be a first-order linearizing Lissajous orbit with constant altitude. The key is that the amplitude of the orbit must be small (on the order of a few thousand kilometers) and the orbital dynamics are not affected by the attitude dynamics for the linear orbital model to be valid. As a consequence, the orbit equations are only effective in the neighborhood of the libration points. However, when the required operating amplitude of the orbit is large, such as in a larger halo orbit, a linear orbital model cannot properly compensate for the nonlinearities in the system, and the need to take into account the nonlinearities becomes increasingly important. Zhao and Cai [24] studied the uncontrolled nonlinear coupling dynamics of multitethered satellite formations (HAS model) in the larger periodic halo orbits based on the Hill's restricted three-body problem (HRTBP), assuming that the masses of the subsatellites were much smaller than the mass of the parent satellite. However, the validity of this assumption depends on the mass ratio between the subsatellites and the parent satellite. If this ratio is small, the approximation is a good one. As the subsatellite mass increases, the nonlinear gravitational terms of each subsatellite should be taken into account.

From the dynamical point of view, tethered dynamic formations near libration points can be broken into four scenarios: launch and transfer to libration orbits, deployment into initial formation, a stationkeeping stage, and reconfiguration into new formation. In [23,24], it was assumed that the system was in the stationkeeping stage, and the tether length was fixed at all times. However, in the proposed interferometry observatory, to completely sample the area spanned by the formation, the systems are required to spiral about the main optical axis, and this can be accomplished by slowly changing the tether lengths. Based on Gates's model [19], Kim and Hall [25] studied the control of rotating variable-length tethered systems for use in several possible SPECS mission scenarios. Again, gravity and other environmental forces were not taken into account, and the tethered system was not considered to be in any libration point orbit. Wong and Misra [26] examined the planar dynamics of a multitethered system with variable-length tethers near the second sun–Earth libration point in the CRTBP. Two simple tether-length laws and a set of spiral motion laws were used to perform the numerical simulations. It was also assumed that the parent mass was located very close to the libration points. In this paper, the three-dimensional reconfiguration dynamics of the static formations near L_2 and the dynamic formations in the larger periodic orbits are investigated by numerical simulations, using a new HRTBP-based formulation.

The paper is organized as follows. First, the assumption of the small mass ratio in [24] is discarded, while the gravitational force acting on each subsatellite is included. An extended HAS model that permits an additional degree of freedom to take into account a variable-length tether during the reconfiguration stage is proposed. A constant-length tether during stationkeeping is treated as a particular case. Based on the HRTBP, a new formulation for the analysis of the dynamics of a multitethered system near collinear libration points is developed for both the stationkeeping stage and the reconfiguration stage. Subsequently, the equilibrium positions and stability analysis for tethered static formations with nonrotating tethers are presented when the parent satellite is located very close to the second libration point. Finally, the coupling dynamics between the rotating tethers and the orbital motion of the tethered dynamic formations are studied using the full nonlinear and time-varying equations of motion when the parent satellite is in larger periodic halo orbits. The effects of the tethers' deployment and retrieval on the system response are investigated with numerical examples.

II. Dynamic Model

A. Description of the System

The coupling dynamics of tethered systems in larger halo orbits is a complex problem. Some of the issues, such as the changing scale of the problem, provide challenges to numerical computations [2]. For instance, the baseline halo orbit has y amplitudes on the order of 700,000 km, whereas the diameter of the formation is a mere 100 m. Also, the velocity of the satellites relative to each other is typically a few meters per hour, whereas their relative speeds to the halo orbit are several thousand kilometers per hour. The successful management of these conflicting requirements is very important to the simulations. In this paper, we develop our orbital model based on the HRTBP. The HRTBP is a simplified version of the CRTBP. As compared with the more widely used CRTBP, the HRTBP has the advantage of a simple and parameterless set of equations, with the presence of symmetries that simplify the numerical computations [22,27]. The HRTBP model is well suited to represent the motion of a satellite around collinear libration orbits near the Earth, and the Hill formulation allows a much simpler description of the dynamics and provides an excellent approximate solution. For applications to the sun–Earth system, the relative error introduced by the use of the Hill approximation, as compared with the CRTBP, is on the order of 1.5% [28]. More details on the HRTBP can be found in [27,28].

A schematic model of the multitethered satellite formation in the required halo orbit treated in the present paper is illustrated in Fig. 1. The ith end satellite is connected to the parent by a tether of variable-length L_{di}. It is assumed that all the masses can be treated as point

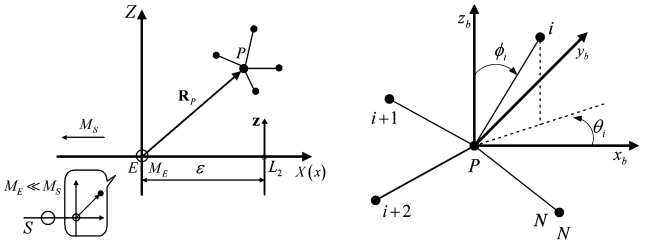

a) b)

Fig. 1 Schematic model of the formation system: a) multitethered satellite in the HRTBP and b) definition of tether angles.

masses, and the tethers are inextensible, always kept taut, and of negligible mass. Because we are interested in basic dynamic features of a multitethered formation for space interferometry, for which the tethers are not too long (the maximum sampling baseline of SPECS mission is 1 km) and made of very light materials [11], the massless tether model can be considered as the best compromise between mathematical complexity of the analytical model and the significance of the model. It is noted that the mass of the tether should be included in the model to obtain more accurate simulations when very long tethers are involved.

In the HRTBP, the motion of the system is described using a set of body-centered rotating coordinates $E - XYZ$ (denoted by S_E) with the origin at the Earth and the X axis in the direction of the sun to the Earth. The Y axis is perpendicular to the X axis in the plane of motion of the primary bodies, and the Z axis is along the normal to this plane. The unit vectors along the X, Y, and Z axes are denoted by $\hat{\mathbf{i}}$, $\hat{\mathbf{j}}$, and $\hat{\mathbf{k}}$, respectively. Halo orbits centered at L_2 are described using an additional set of coordinates $L_2 - xyz$ (denoted by S_L), with the origin at the second libration point and otherwise being parallel to S_E.

Using a spherical coordinate system centered at the parent satellite, the in-plane and out-of-plane rotation angles θ_i and ϕ_i are measured relative to the x_b, y_b, and z_b axes (denoted by S_P, and parallel to x, y, and z axes, respectively) (Fig. 1b). The angle θ_i is measured counterclockwise from the x_b axis about the z_b axis, and ϕ_i is measured relative to the positive z_b axis. At any arbitrary instant, the location of the ith end satellite relative to the parent satellite can be described as

$$x_i^b = L_{di}\cos\theta_i \sin\phi_i; \qquad y_i^b = L_{di}\sin\theta_i \sin\phi_i; \qquad z_i^b = L_{di}\cos\phi_i \tag{1}$$

The position vector of the parent satellite relative to the Earth in S_E is denoted by $\mathbf{R}_P$, while the position vector of the end satellite m_i in S_P is denoted by $\mathbf{r}_i$. These vectors are given by

$$\mathbf{R}_P = X\hat{\mathbf{i}} + Y\hat{\mathbf{j}} + Z\hat{\mathbf{k}} \tag{2}$$

$$\mathbf{r}_i = x_i^b\hat{\mathbf{i}} + y_i^b\hat{\mathbf{j}} + z_i^b\hat{\mathbf{k}} \tag{3}$$

$3N + 3$ generalized coordinates X, Y, Z, θ_i, ϕ_i, and L_{di} for $i = 1, 2, \ldots, N$ are involved, where X, Y, and Z are the coordinates of the parent satellite relative to the Earth in S_E, while θ_i ,ϕ_i (the in-plane and the out-of-plane angles), and L_{di} define the orientation and position of the end satellite, m_i.

B. Derivation of the Equations of Motion

The equations of motion of the system are deduced in the framework of the Lagrangian formulation. The velocity vectors of the parent and end satellites are given by

$$\mathbf{v}_P = \dot{\mathbf{R}}_P + \boldsymbol{\omega} \times \mathbf{R}_P \tag{4}$$

$$\mathbf{v}_i = \mathbf{v}_P + \dot{\mathbf{r}}_i + \boldsymbol{\omega} \times \mathbf{r}_i \tag{5}$$

where the dot represents the time derivative in the rotating frame, $\boldsymbol{\omega} = n\hat{\mathbf{k}}$, and $n = 1.99099 \times 10^{-7}$ rad/s for the sun–Earth system. The kinetic energy term of the formation system is given by

$$T_f = \frac{1}{2}m_P\mathbf{v}_P \cdot \mathbf{v}_P + \frac{1}{2}\sum_{i=1}^{N} m_i\mathbf{v}_i \cdot \mathbf{v}_i \tag{6}$$

The potential energy term of the multitethered satellite formation in the HRTBP [28] is given by

$$E_g = -m_P\left[\frac{\mu_e}{|\mathbf{R}_P|} + \frac{1}{2}n^2(3X^2 - |\mathbf{R}_P|^2)\right] - \sum_{i=1}^{N} m_i\left\{\frac{\mu_e}{|\mathbf{R}_P + \mathbf{r}_i|} + \frac{1}{2}n^2[3(X + x_i^b)^2 - |\mathbf{R}_P + \mathbf{r}_i|^2]\right\} \tag{7}$$

It is assumed that the length of the tethers is small when compared with the orbital altitude of the tethered system, implying that $|\mathbf{r}_i|$ is small when compared with $|\mathbf{R}_P|$. Expanding $(\mathbf{R}_P + \mathbf{r}_i)^{-1}$ in Eq. (7) in a binomial series and neglecting terms of the order of four and higher, one obtains

$$\frac{1}{|\mathbf{R}_P + \mathbf{r}_i|} \approx \frac{1}{R_P}\left\{1 - \frac{\boldsymbol{\rho} \bullet \mathbf{u}_i L_{di}}{R_P} + \frac{1}{2}\frac{[3(\boldsymbol{\rho} \bullet \mathbf{u}_i)^2 - \mathbf{u}_i \bullet \mathbf{u}_i]L_{di}^2}{R_P^2}\right\} \tag{8}$$

where $R_P = |\mathbf{R}_P|$, $\boldsymbol{\rho}$ is the unit vector along $\mathbf{R}_P$, and $\mathbf{u}_i$ is the unit vector along $\mathbf{r}_i$.

Using the kinetic energy term and the potential term given by Eqs. (6) and (7), Lagrange's equations can be applied by

$$\frac{\mathrm{d}}{\mathrm{d}t}\left(\frac{\partial T_f}{\partial \dot{q}}\right) - \frac{\partial T_f}{\partial q} + \frac{\partial E_g}{\partial q} = Q_q^F \tag{9}$$

where $q = X, Y, Z, \theta_i, \phi_i, L_{di}$, respectively.

For the convenience of analysis, a set of nondimensional quantities are defined as

$$\hat{X} = X/\ell; \qquad \hat{Y} = Y/\ell; \qquad \hat{Z} = Z/\ell; \qquad \hat{L}_{di} = L_{di}/\ell;$$
$$\ell = (\mu_e/n^2)^{1/3}; \qquad \tau = nt; \qquad \mu_i = m_i/m; \qquad m = m_P + \sum_{i=1}^{N} m_i \tag{10}$$

where ℓ and τ are the scales of length and time in the HRTBP [27].

In this paper, we focus on a multitethered satellite system around L_2, using the transformation in the new coordinate system $L_2 - xyz(S_L)$ and a similar transformation for the tether lengths. The coordinates of L_2 in S_E are $(\varepsilon, 0, 0)$:

$$x = (\hat{X} - \varepsilon)/\varepsilon; \qquad y = \hat{Y}/\varepsilon; \qquad z = \hat{Z}/\varepsilon; \qquad l_{di} = \hat{L}_{di}/\varepsilon \tag{11}$$

Substituting Eqs. (1–8), (10), and (11) into Eq. (9) and performing the required differentiations, the nondimensional equations of motion for the parent satellite can be expressed as

$$x'' - 2y' - (3 - 1/r_P^3)(1 + x) + \sum_{i=1}^{N} F_{xi} = \frac{Q_X^F}{mn^2\ell\varepsilon} \tag{12a}$$

$$y'' + 2x' + y/r_P^3 + \sum_{i=1}^{N} F_{yi} = \frac{Q_Y^F}{mn^2\ell\varepsilon} \tag{12b}$$

$$z'' + (1 + 1/r_P^3)z + \sum_{i=1}^{N} F_{zi} = \frac{Q_Z^F}{mn^2\ell\varepsilon} \tag{12c}$$

Similarly, the nondimensional equations of the ith tether are given as

$$\theta_i'' l_{di}^2 \sin^2\phi_i + (y''\cos\theta_i - x''\sin\theta_i) l_{di}\sin\phi_i + \phi_i'(1+\theta_i') l_{di}^2 \sin 2\phi_i + [2(x'\cos\theta_i + y'\sin\theta_i) + 3(x+1)\sin\theta_i] l_{di}\sin\phi_i + \frac{3}{2} l_{di}^2 \sin^2\phi_i \sin 2\theta_i + \lambda_{\theta_i} + 2 l_{di}(\theta_i'+1) l_{di}' \sin^2\phi_i = \frac{Q_{\theta_i}^F}{m_i n^2 \ell^2 \varepsilon^2} \tag{13a}$$

$$l_{di}^2 \phi_i'' + (\cos\theta_i x'' + \sin\theta_i y'') l_{di}\cos\phi_i - (z''+z) l_{di}\sin\phi_i + [2(x'\sin\theta_i - y'\cos\theta_i) - 3(x+1)\cos\theta_i] l_{di}\cos\phi_i - \frac{1}{2}[(1+\theta_i')^2 + 3\cos^2\theta_i] l_{di}^2 \sin 2\phi_i + \lambda_{\phi_i} + 2 l_{di}\phi_i' l_{di}' = \frac{Q_{\phi_i}^F}{m_i n^2 \ell^2 \varepsilon^2} \tag{13b}$$

$$l_{di}'' + (x''\cos\theta_i + y''\sin\theta_i)\sin\phi_i + (z''+z)\cos\phi_i + [2(x'\sin\theta_i - y'\cos\theta_i) - 3(x+1)\cos\theta_i]\sin\phi_i - (3\cos^2\theta_i \sin^2\phi_i - 1) l_{di} - [(\theta_i'+1)^2 \sin^2\phi_i + \phi_i'^2] l_{di} + \lambda_{l_{di}} = \frac{Q_{L_{di}}^F}{m_i n^2 \ell \varepsilon} \tag{13c}$$

where the prime denotes differentiation with respect to the nondimensional time τ, $r_P = \varepsilon\sqrt{(1+x)^2 + y^2 + z^2}$, and Q_X^F, Q_Y^F, Q_Z^F, $Q_{\theta_i}^F$, $Q_{\phi_i}^F$, and $Q_{L_{di}}^F$ are the generalized forces that can be control forces or other perturbations, such as those associated with moon gravitation. The components of the unit vectors $\tilde{\boldsymbol{\rho}}$, $\mathbf{u}_i$, as well as the tether influence terms F_{xi}, F_{yi}, and F_{zi}, are given in Appendix A. The expressions for λ_{θ_i}, λ_{ϕ_i}, and $\lambda_{l_{di}}$ in Eq. (13) are listed in Appendix B. If there is no perturbation of subsatellites and all of the generalized forces are equal to zero, a degenerate form of Eq. (12) corresponds to the uncontrolled dynamic equations of single spacecraft around L_2 in the HRTBP [27].

The equations derived previously, which govern the dynamics of multitethered formation near L_2, are highly nonlinear. They can be used with any kind of tethered systems (static formation with nonrotating tethers at L_2, dynamic formation with rotating tethers on periodic orbits, stationkeeping with constant length, or reconfiguration with variable length). Next, some insight can be obtained from equilibrium positions and an approximate analysis of the linearized equations for static formation with nonrotating tethers at L_2. Numerical studies of the full nonlinear equations would illustrate the behavior of dynamic formation with rotating tethers on periodic orbits around L_2 under some special conditions during both the stationkeeping and reconfiguration stages.

III. Stability of Static Formations at L_2

The questions of the dynamics and the stability of tethered static formations with nonrotating tethers when the parent satellite is located very close to L_2 are now addressed. Furthermore, the system's stability during reconfiguration is also investigated using numerical methods.

A. Equilibrium Positions and Linearized Equations

It is assumed that there are no additional perturbations or control forces on the system. Also, because the tether lengths are constants, the length in Eq. (13c) is not required. The equations determining the equilibrium positions [that is, the steady-state solutions of Eqs. (12), (13a), and (13b)] are

$$-(3 - 1/r_P^3)(1+x) + \sum_{i=1}^{N} \mu_i \{ l_{di}(\cos\theta_i \sin\phi_i - f_{i1}) + g_{i1} \} = 0 \tag{14}$$

$$y/r_P^3 + \sum_{i=1}^{N} \mu_i \{ -l_{di} f_{i2} + g_{i2} \} = 0 \tag{15}$$

$$(1 + 1/r_P^3) z + \sum_{i=1}^{N} \mu_i \{ l_{di}(\cos\phi_i - f_{i3}) + g_{i3} \} = 0 \tag{16}$$

$$3(1+x) l_{di} \sin\theta_i \sin\phi_i + 3 l_{di}^2 \sin^2\phi_i \sin\theta_i \cos\theta_i + \lambda_{\theta_i} = 0 \tag{17}$$

$$-3(x+1) l_{di}\cos\theta_i \cos\phi_i - z l_{di}\sin\phi_i - l_{di}^2 \sin\phi_i \cos\phi_i (1 + 3\cos^2\theta_i) + \lambda_{\phi_i} = 0 \tag{18}$$

where f_{ij} and $g_{ij} (j = 1, 2, 3)$ are given in Appendix A.

Instead of a selective search, in this paper, the analysis of multitethered formations is focused on the most important case [21–23]. A set of values and the equation of x_e are given by

$$-[3(1+x_e) - C_0] + \sum_{i=1}^{N} \mu_i \{ [1 + 2C_1](-1)^{i-1} l_{di} + 3C_2 l_{di}^2 \} = 0 \tag{19}$$

$$y_e = z_e = 0 \tag{20}$$

$$\theta_{ie} = (i-1)\pi; \qquad \phi_{ie} = \pi/2 \tag{21}$$

where x_e, y_e, z_e, θ_{ie}, and ϕ_{ie} denote the values of the equilibrium positions, $C_0 = \varepsilon^{-3}/(1+x_e)^2$, $C_1 = \varepsilon^{-3}/(1+x_e)^3$, $C_2 = \varepsilon^{-3}/(1+x_e)^4$, and $\varepsilon = (1/3)^{1/3}$ in the normalized setting. Expanding $1/(1+x_e)^2$, $1/(1+x_e)^3$, and $1/(1+x_e)^4$ in a binomial series, neglecting terms of the order of three and higher, and solving Eq. (19) for x_e, the result is

$$x_e = \frac{\sum_{i=1}^{N} \mu_i \{ 7(-1)^{i-1} l_{di} + 9 l_{di}^2 \}}{9 + 18 \sum_{i=1}^{N} \mu_i \{ (-1)^{i-1} l_{di} + 2 l_{di}^2 \}} \tag{22}$$

The preceding values describe a particular equilibrium configuration, with the tethers aligned with the x axis. The distance between the parent mass and L_2 depends on factors such as the mass ratios, the tether lengths, and the number of end masses. Equation (22) takes the much simpler form:

$$x_e = \frac{\mu_1 l_{d1}^2 + \mu_2 l_{d2}^2}{1 + 4(\mu_1 l_{d1}^2 + \mu_2 l_{d2}^2)} \tag{23}$$

for the equilibrium position of a three-satellite case with a symmetrical configuration ($N = 2$, $\mu_1 = \mu_2 = \mu$, and $l_{d1} = l_{d2} = l_d$). As seen in Eq. (23), there is no excursion from L_2 for the parent satellite when $l_d = 0$. As the tether lengths or mass ratios increase, the distance between the equilibrium position of the parent satellite and L_2 increases, and the equilibrium position of the parent satellite always stays on the right side of $L_2 (x_e > 0)$.

Multitethered satellites, such as static formations, are stabilized by gravity gradient torques and are generally expected to be operated around the equilibrium positions. Therefore, the dynamic characteristics about the equilibrium positions have to be investigated. The equilibrium positions corresponding to the solution summarized in Eqs. (20–22) are considered. It is assumed that the tether lengths are constant, and the deviations of the parent satellite and subsatellites from the equilibrium positions are small.

Defining $x = x_e + \delta x$, $y = y_e + \delta y$, $z = z_e + \delta z$, $\theta_i = \theta_{ie} + \delta\theta_i$, and $\phi_i = \phi_{ie} + \delta\phi_i$, substituting them into Eqs. (12) and (13), expanding $1/r_p^3$, $1/r_p^4$, and $1/r_p^5$ in a binomial series, and neglecting terms of order of two and higher-order small perturbations, the linearized equations of the ith subsatellite are obtained to be

$$\delta\theta_i'' + \{3 + 3C_1 + (-1)^{i-1}[3(x_e + 1) - C_0]/l_{di}\}\delta\theta_i + (-1)^{i-1}(\delta y'' + 2\delta x' + C_1\delta y)/l_{di} - 3C_2\delta y = 0 \quad (24)$$

$$\delta\phi_i'' + \{4 + 3C_1 + (-1)^{i-1}[3(x_e + 1) - C_0]/l_{di}\}\delta\phi_i - \delta z''/l_{di} + [3C_2(-1)^{i-1} - (C_1 + 1)/l_{di}]\delta z = 0 \quad (25)$$

where $C_3 = \varepsilon^{-3}/(1 + x_e)^5$.

As x_e is very small ($C_1 \approx 3$), the libration frequencies of the tethers are approximately $\sqrt{3 + 3C_1}n \approx 3.46n$ for in-plane motion and $\sqrt{4 + 3C_1}n \approx 3.60n$ for out-of-plane motion. These computational results are very close to those given in [23] ($3.43n$ and $3.58n$), and the errors are introduced by the use of the Hill's approximation.

If the motions are not small, the libration frequencies could be different due to the coupling between the tether librations and the motion of the parent satellite. Once the motion of the parent mass is sufficiently large, the nonlinear effects become significant, resulting in a change of frequencies. In fact, the nonlinear coupling dynamics can be studied by numerical methods. In the following parts, the stability analysis of tethered static formations is simulated numerically using Gears's method (ODE15s in MATLAB) for the stiff, nonlinear, and coupled ordinary differential equations (ODEs) (13), (13a), and (13b). This analysis is performed for both a stationkeeping stage with constant-length tethers and a reconfiguration stage with variable-length tethers. The options in the MATLAB code are written to obtain a relative error of 1×10^{-13} and an absolute error of 1×10^{-16}. The accuracy of the numerical solution is assessed by using two different ways. First, the same solver (ODE15s) is used with the bigger error tolerances [relative tolerance (RelTol), $1e-6$; absolute tolerance (AbsTol), $1e-8$]. Second, other solvers (ODE45/ODE113 in MATLAB) are used with the small error tolerances (RelTol, $1e-13$; AbsTol, $1e-16$). Because the solutions from ODE15s match those obtained from different solver/error tolerances and are almost indistinguishable at the level of the plot, the solutions are considered acceptable. Consequently, only the solutions from ODE15s with small error tolerances are shown in the next figures.

B. Stability Analysis During Stationkeeping

For the sake of simplicity, it is assumed that the multitethered system is the three-satellite case with a symmetrical configuration ($N = 2$, $\mu_1 = \mu_2 = \mu$, and $l_{d1} = l_{d2} = l_d$). Small initial deviations from θ_{ie} and ϕ_{ie} are considered, where the initial out-of-plane angles are $\phi_1(0) = 85$ deg and $\phi_2(0) = 95$ deg, and the in-plane angles are $\theta_1(0) = 5$ deg and $\theta_2(0) = 185$ deg The parent satellite is initially displaced by x_e from L_2 in the x direction, with no excursions in the y and z directions. The equilibrium position x_e can be obtained from Eq. (23).

For a given mass ratio ($\mu = 1/3$), Fig. 2a shows that the tether length has some impact on the stability of the parent satellite. Two different tether lengths, $L_d = 100$ km and $L_d = 10$ km, are considered. For a given tether length ($L_d = 10$ km), Fig. 2b shows that the mass ratio also has some impact on the stability of the parent satellite. It can be seen that longer tether lengths and big mass ratios make the parent satellite move away from its equilibrium position earlier; in other words, the motion of the parent satellite is more unstable for larger initial equilibrium position x_e. Figure 3 shows the attitude stability of static formations under different tether lengths and different mass ratios. It can be seen that the solutions from $\mu = 1/3$ and $L_d = 100$ km match those obtained from $\mu = 1/3$ and $L_d = 10$ km, and $\mu = 1/1000$ and $L_d = 10$ km and are almost indistinguishable at the level of the plot. Consequently, the change of x_e has almost no impact on in-plane or out-of-plane tether librations when the parent satellite is located very close to L_2. The numerical results are consistent with the analytical estimation, using linearized equations (23–25).

C. Stability Analysis During Reconfiguration

During the reconfiguration stage, an additional degree of freedom is introduced by making the tether length variable. It is assumed that

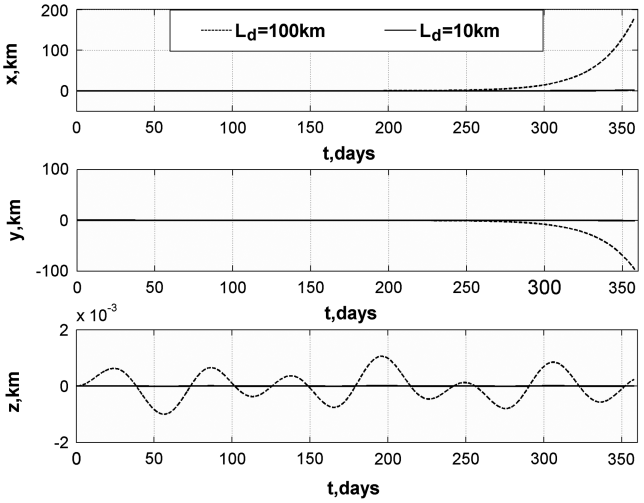

a) Displacement under different tether lengths

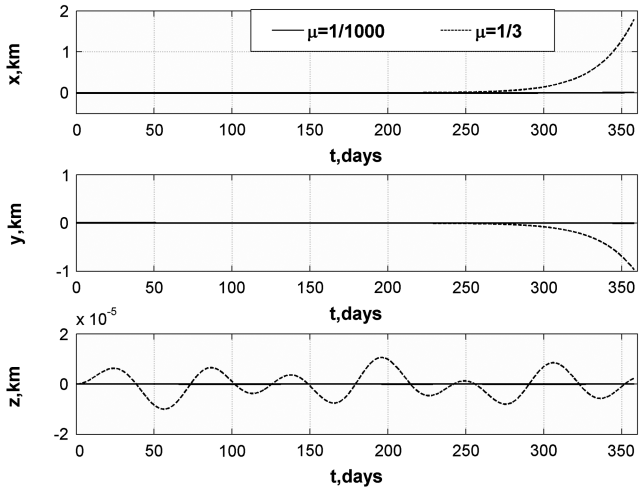

b) Displacement under different mass ratios

Fig. 2 Parent satellite stability of static formations.

the tether-length rate is constant. The tether-length, length rate, and length acceleration functions take the form [26]

$$l_{di} = l_{0,di} + \lambda_C\tau,\ l_{di}' = \lambda_C,\ l_{di}'' = 0 \quad (26)$$

where $l_{0,di}$ is the initial length of the ith tether, and λ_C is a dimensionless constant. The tether is extending when λ_C is greater than zero and retracting if λ_C is negative. An example of the length change over time can be seen in Fig. 4. During deployment, the tether lengths increase, according to Eq. (26), from an initial length of 10 km to a final length of 50 km. During retrieval, the tether lengths decrease, according to Eq. (26), from an initial length of 50 km to a final length 10 km, and the nondimensional reconfiguration time is about 0.8909 (51.6 days) for deployment with $\lambda_C = 3 \times 10^{-5}$ and retrieval with $\lambda_C = -3 \times 10^{-5}$. Once the final length is reached, the tether lengths are then held constant for the stationkeeping stage.

A three-satellite case with variable-length tethers ($N = 2$ and $\mu_1 = \mu_2 = 1/3$) is considered for the reconfiguration stage. The other initial parameters are the same as those during the stationkeeping stage. Substituting Eq. (26) into Eqs. (12), (13a), and (13b), nonlinear numerical simulations are performed using the nonlinear equation in order to study the stability of tethered static formations during the reconfiguration stage under the constant tether law, shown in Fig. 4.

The stability during deployment under the constant tether law can be seen in Fig. 5, in which the tether lengths increase with the time until the final lengths are reached. As shown in Fig. 5a, the parent satellite moves away from its initial position along the negative

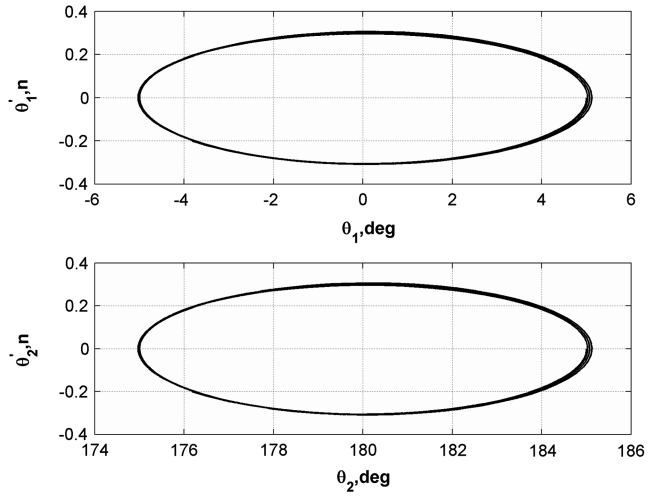

a) Phase portrait of in-plane tether librations

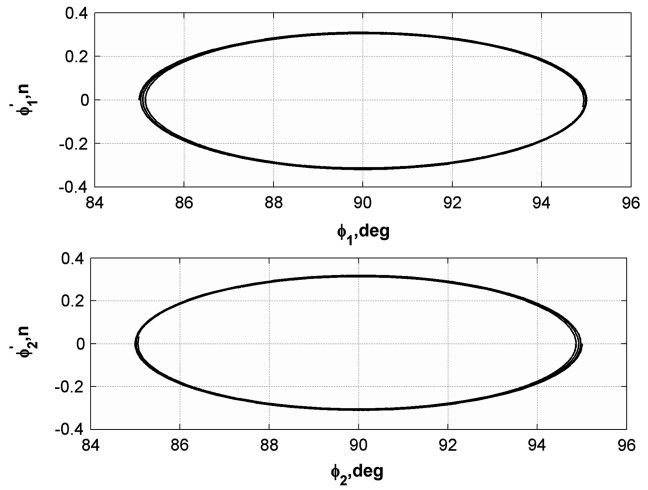

b) Phase portrait of out-of-plane tether librations

Fig. 3 Attitude stability of static formations.

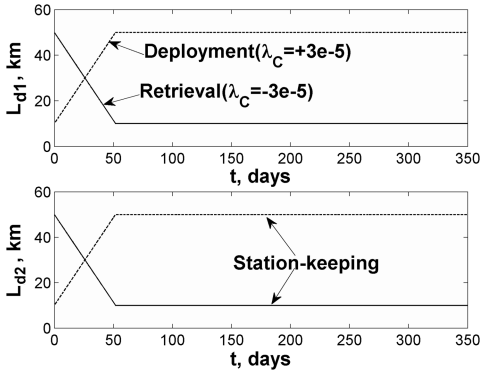

Fig. 4 Linear tether law with $\lambda_C = \pm 3 \times 10^{-5}$.

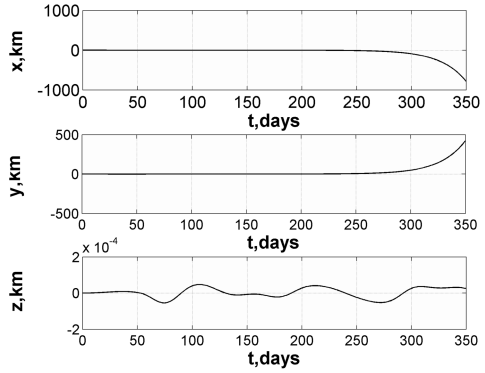

a) Displacement of parent satellite

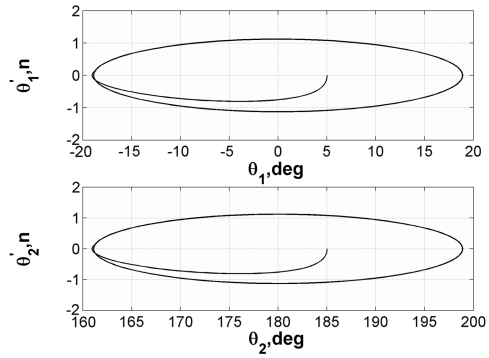

b) Phase portrait of in-plane tether librations

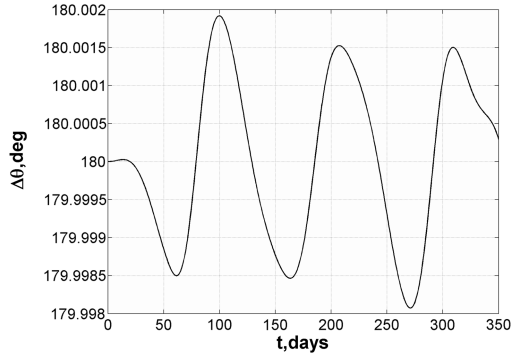

c) In-plane relative angle ($\Delta\theta$=θ_2-θ_1)

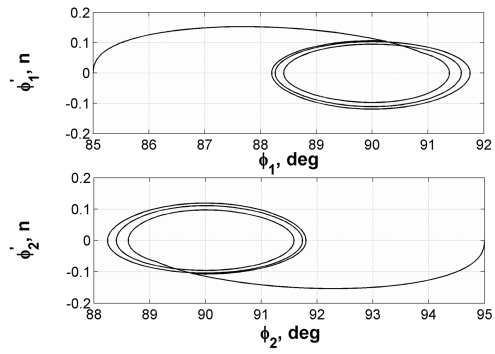

d) Phase portrait of out-of-plane tether librations

Fig. 5 Stability during deployment under the constant tether law ($\lambda_C = 3 \times 10^{-5}$).

direction of the x axis and the positive direction of the y axis after some days, with a very small excursion along the z axis. It can be seen that the in-plane and out-of-plane tether librations are stable (see Figs. 5b and 5d), and the system remains in its initial configuration (see Fig. 5c) in the stationkeeping stage that follows after deployment.

The stability during retrieval under the constant tether law can be seen in Fig. 6. Here, the tether lengths decrease with the time until the final lengths are reached. As shown in Fig. 6a, the parent satellite also moves away from its initial position along all three axes after some days, and the excursions are larger than those during deployment. It can be seen that the in-plane tether librations will depart from their initial positions, because the in-plane angles increase with time (see Fig. 6b). The in-plane relative angle changes within a range of about ± 6 deg from the equilibrium points (see Fig. 6c), which is larger than that during deployment. Additionally, the change of out-of-plane librations is too large to remain in the planar

configuration for tethered formations with an initial retrieval stage (see Fig. 6d).

Although tethered static formations near libration points may have more advantages than free formations [23,24], the nonspinning case will lead to a subsatellite dynamics dominated by gravitational effects, with very little stiffening of the tethers. Consequently, such a configuration is likely to experience difficulties with slack tethers.

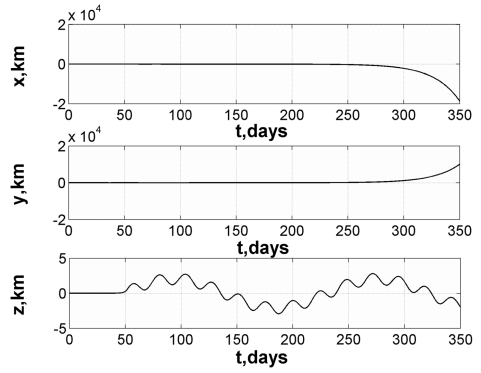

a) Displacement of parent satellite

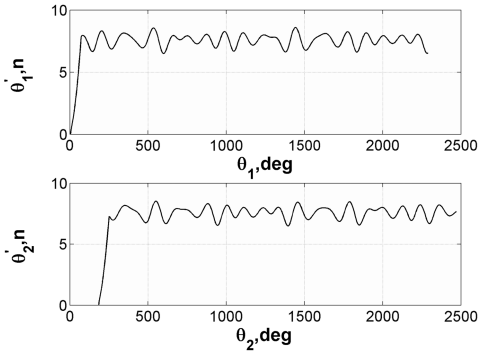

b) Phase portrait of in-plane tether librations

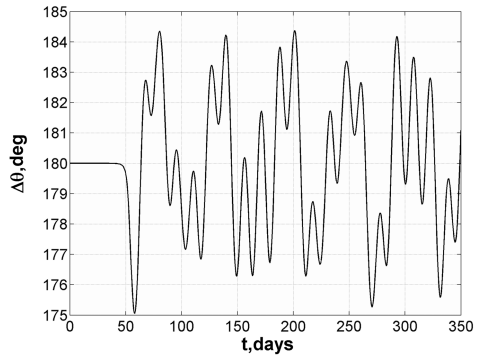

c) In-plane relative angle ($\Delta\theta=\theta_2-\theta_1$)

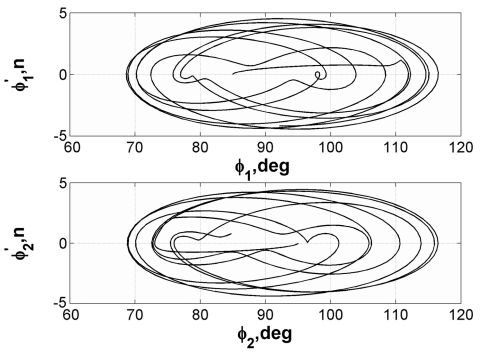

d) Phase portrait of out-of-plane tether librations

Fig. 6 Stability during retrieval under the constant tether law ($\lambda_C = -3 \times 10^{-5}$).

Therefore, a spin is necessary to provide centrifugal stiffening of the tethers and keep the system in its configuration, especially for a deep-space interferometry mission on larger periodic orbits.

IV. Stability of Dynamic Formations on Periodic Orbits

Practically, exact libration points are unsuitable for missions, because radio signals from the satellite would disappear in solar noise. Therefore, libration point missions are not located directly at the libration points but in a quasi-periodic (Lissajous) orbit or periodic orbit (halo) around the libration point. For instance, the SPECS will be located on the halo orbit. We focus on the coupling dynamics of formation systems in larger halo orbits during both stationkeeping and reconfiguration stages. The three-dimensional dynamics of tethered dynamic formations are simulated using the same numerical method as the static formation for Eqs. (12), (13a), and (13b).

A. Computation of Halo Orbits near L_2 in Hill's Restricted Three-Body Problem

To investigate the coupling dynamics of spinning multitethered formations in larger halo orbits, the halo orbits themselves need to be obtained. Halo orbits are attained only when amplitudes A_x and A_z are large enough that nonlinear contributions make the in-plane and out-of-plane frequencies the same. The minimum A_x of halo orbits around L_2 in sun–Earth system is 200,000 km. The nondimensional initial conditions that lead to accurate halo orbits around L_2 in the HRTBP can be obtained by a nondimensional process, coordinate transformation, and a differential correction process [29,30]. Three sets of initial conditions of halo orbits near L_2 in the HRTBP are shown in Table 1, where $y(0) = x'(0) = z'(0) = 0$, and T denotes the orbit period.

Another example of a halo orbit is chosen from rough data from either the Genesis or Solar and Heliospheric Observatory (SOHO) missions. This orbit is roughly 1,200,000 km from the Earth, in the opposite direction of sun, and the orbit radius is roughly 280,000 km for a projectile traveling roughly 0.350 km/s. Using the same methods, the nondimensional initial conditions can be obtained to be $x(0) = -0.198127$, $z(0) = \pm 0.179589$, $y'(0) = 1.088221$, and $z(0) > 0$ for the northern halo orbit and $z(0) < 0$ for the southern halo orbit. The period of this orbit is 178.85 days.

B. Stability of System During the Stationkeeping Stage

Let us consider the stationkeeping stage with constant-length tethers, which is a particular case of the reconfiguration stage when the terms proportional to the nondimensional length rate l'_{di} and acceleration l''_{di} in Eqs. (12) and (13) are equal to zero. If there is no special instruction, the tether length is always 0.2 km during the stationkeeping stage. The numerical results for the attitude stability under different halo orbits are shown to illustrate the impact of orbital amplitudes and directions. Moreover, the impact of the mass ratio on the stability of the system is demonstrated. It should be noted that the orbits are uncontrolled and without initial injection error here. For convenience of computation, we also focus on the three-satellite constellation case.

1. Stability Under Different Halo Orbit Amplitudes and Directions

It is important to know how the motions of the parent satellite affect the tether librations of the spinning system. Wong and Misra [23] presented how the tether librations were affected by the

Table 1 Initial condition of three halo orbits near L_2 in the HRTBP

A_z (km)	T (days)	$x(0)$	$z(0)$	$y'(0)$
200,000	179.019	−0.177286	0.118246	1.019281
400,000	178.659	−0.222130	0.229499	1.165691
600,000	177.964	−0.292768	0.328974	1.383916

amplitudes of orbits in which the parent satellite was prescribed to small first-order linearizing Lissajous orbits. In this paper, it is assumed that the parent satellite is in nonlinear larger halo orbits, and the effects of orbital amplitudes and directions are included. For a given formation configuration ($L_{d1} = L_{d2} = L_d = 0.2$ km and $\mu_1 = \mu_2 = \mu = 1/3$), small initial deviations from ϕ_{ie} are considered, where the initial out-of-plane angles are $\phi_1(0) = 85$ deg and $\phi_2(0) = 95$ deg, and the initial in-plane angular velocity is $\theta_1'(0) = \theta_2'(0) = \theta'(0) = 10n$.

Figure 7a shows the halo orbit stability in about two orbital periods, using the initial conditions of orbits given in Table 1. Figures 7b–7d show the corresponding attitude stability on halo orbits in Fig. 7a, with different amplitudes. It can be seen that the parent satellite does not depart from the required orbit over the relatively long term, and the stability of the in-plane spin (see Fig. 7b) and system configuration (see Fig. 7c) are affected to only a small extent as the orbital amplitudes increase in an appropriate range. The range of out-of-plane librations increases with the increase of the orbit amplitudes (see Fig. 7d).

Figure 8a shows the orbital stability of halo orbits with different directions (northern and southern halo orbits) in two orbital periods using the initial conditions of the orbits of the Genesis or SOHO missions. Figures 8b–8d show the attitude stability under different orbital directions. It can be seen that the orbital directions have very little effect on in-plane tether angular velocities and out-of-plane tether librations; however, the southern halo orbit is more conducive to keeping the system in its lineal configuration when compared with the northern halo orbit (see Fig. 8d).

2. Stability at Different Mass Ratios

Several configurations of spin-stabilized tethered formations have been proposed that possibly meet the needs of space science exploration. These configurations are divided into two basic categories. In the first, the masses of subsatellites are close to the mass of the parent satellite ($m_i \approx m_P$); in the second, the masses of subsatellites are much smaller than the mass of the parent satellite ($m_i \ll m_P$). Zhao and Cai [24] presented the stability of the second category in a larger halo orbit. The orbit stability and attitude stability of the two different categories are compared with each other in the following numerical simulations.

With the given tether length ($L_d = 0.2$ km) and initial spin rate $\theta'(0) = 10n$ of the spinning multitethered satellite formation system, the parent satellite is placed in the southern halo orbit in Fig. 8a. Figure 9 shows that the mass ratio has some impact on the stability of the system. It can be seen in Fig. 9a that the parent satellite will depart from the required orbits after four orbital periods because of the unstable characteristics of the dynamics near the libration points and the coupling between the tether librations and the parent satellite motions. The orbital motion of the system is more stable for the small mass ratio ($\mu = 1/1000$) formation. As the mass ratio decreases, the amplitude of both in-plane tether angular velocities (see Fig. 9b) and out-of-plane librations (see Fig. 9d) decreases, and the configuration of the tethered system is more stable (see Fig. 9c).

C. Stability of the System During the Reconfiguration Stage

It is assumed that the tether lengths are changing at an exponential rate for both deployment and retrieval. The tether length, length rate, and length acceleration functions take the form [26]

$$l_{di} = l_{0,di}e^{\lambda_e \tau},\ l'_{di} = \lambda_e l_{0,di}e^{\lambda_e \tau},\ l''_{di} = \lambda_e^2 l_{0,di}e^{\lambda_e \tau} \qquad (27)$$

where $l_{0,di}$ is the initial length of the ith tether, and λ_e is a dimensionless constant. Again, $\lambda_e > 0$ indicates tether extension. An example of exponential length change over time can be seen in Fig. 10. During deployment, the tether lengths increase, according to Eq. (27), from an initial length of 50 m to a final length of 500 m; during retrieval, the tether lengths decrease, according to Eq. (27), from an initial length of 500 m to a final length of 50 m. The nondimensional reconfiguration time is about 7.6753 (446 days) for deployment with $\lambda_e = 0.3$ and retrieval with $\lambda_e = -0.3$. Once the final length is reached, the tether lengths are then held constant for the stationkeeping stage.

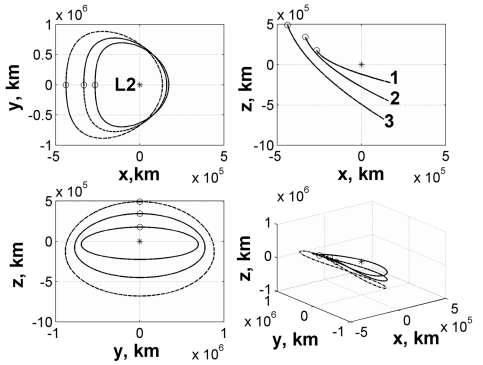

a) Three Halo orbits centered about Sun-Earth L2

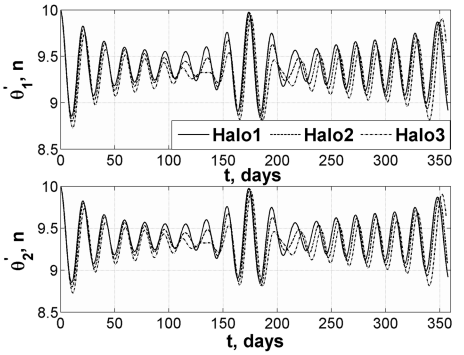

b) In-plane tether angular velocities

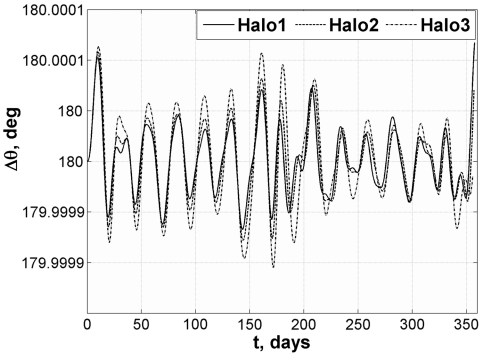

c) In-plane relative angle ($\Delta\theta$=θ_2-θ_1)

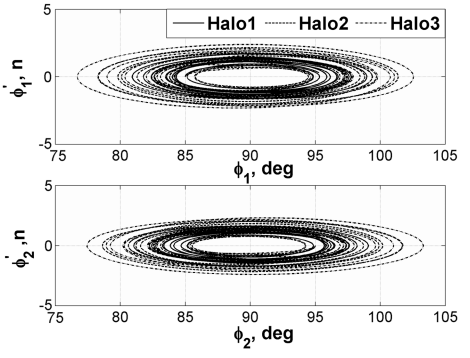

d) Phase of portrait out-of-plane tether librations

Fig. 7 Orbit and attitude stability under different amplitudes of orbits.

Next, the reconfiguration stability analysis of dynamic formations with variable-length tethers in larger halo orbits is studied. It is assumed that the parent satellite is predefined on the southern halo orbit in Fig. 8a for initial in-plane angular velocities $\theta'(0) = 30n$ and the three-satellite case ($\mu_1 = \mu_2 = 1/3$), without control forces and initial injection errors considered. If tether lengths are changing at an

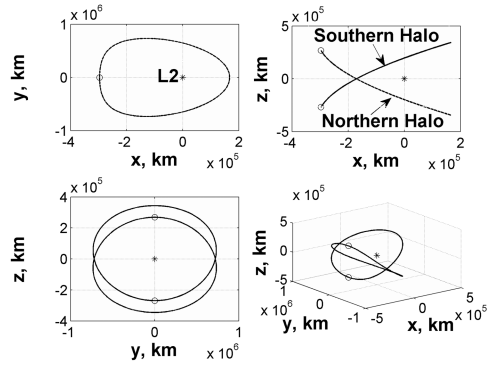

a) Northern Halo orbit and Southern Halo orbit

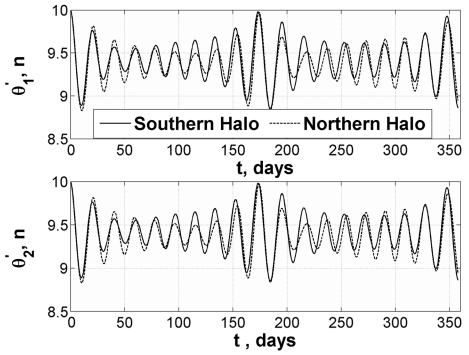

b) In-plane tether angular velocities

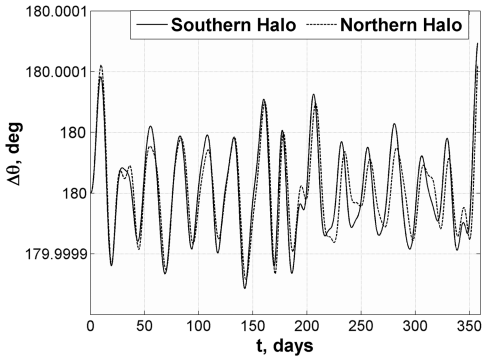

c) In-plane relative angle ($\Delta\theta=\theta_2-\theta_1$)

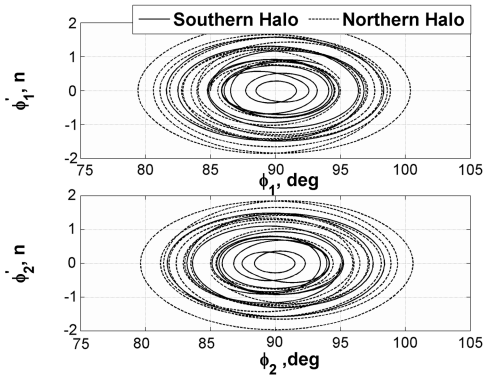

d) Phase portrait of out-of-plane tether librations

Fig. 8 Orbit and attitude stability under different directions of orbit.

exponential rate, as in the deployment and retrieval stages, the terms proportional to the nondimensional length rate l'_{di} and acceleration l''_{di} in Eqs. (12) and (13) are different from zero. Substituting Eq. (27) into Eqs. (12), (13a), and (13b), nonlinear numerical simulations can be performed using the nonlinear equation for both deployment and retrieval.

Figure 11 shows the stability of the system when the coefficients are positive during deployment, corresponding to an increase in

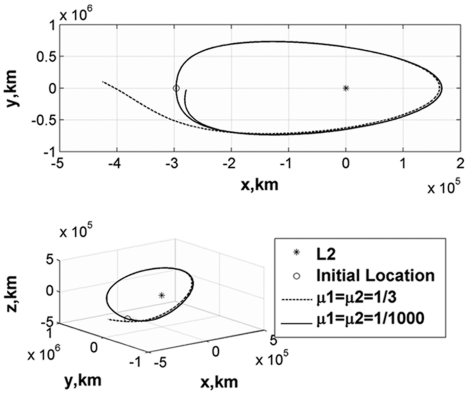

a) Halo orbit motion (4T)

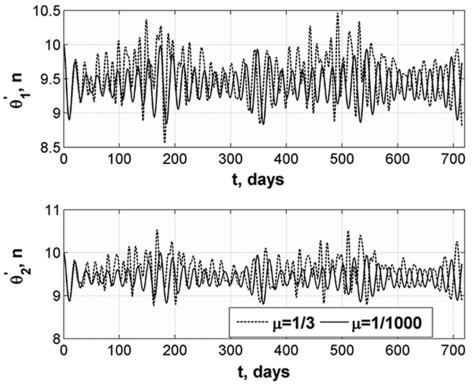

b) In-plane tether angular velocities

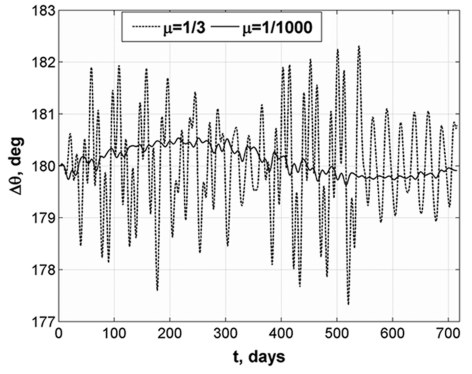

c) In-plane relative angle ($\Delta\theta=\theta_2-\theta_1$)

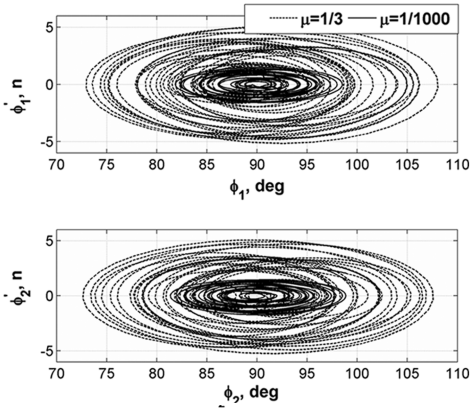

d) Phase portrait of out-of-plane tether librations

Fig. 9 Orbit and attitude stability under different mass ratios.

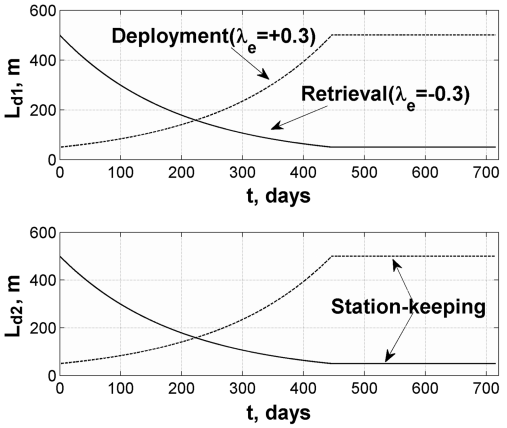

Fig. 10 Exponential tether law with $\lambda_e = \pm 0.3$.

tether lengths with time until the final lengths are reached. The parent satellite departs from the predefined nominal halo orbit after four orbital periods (see Fig. 11a), and the in-plane spin is no longer stable as the in-plane angular velocities decrease to zero during deployment, where the most critical situation is encountered in the last phase of the simulation (see Fig. 11b). Consequently, the tethered system does not maintain its desired initial configuration and is likely to experience difficulties with slack tethers or accidental collision of subsatellites (see Fig. 11c). Therefore, a more controlled effort is required to maintain the desired in-plane angular velocities. As shown in Fig. 11d, the phase portrait of the out-of-plane tether librations illustrates the out-of-plane stability during deployment, in which it can be seen that the librations depart far from their desired positions and the planar configuration ceases to exist.

The stability during retrieval under the exponential tether law can be seen in Fig. 12. Here, the coefficients are negative. The parent satellite also departs from the predefined nominal halo orbit after four orbital periods (see Fig. 12a). The in-plane angular velocities increase from the initial rate ($30n$) to a higher rate (about $3000n$) during the whole retrieval and then remain at this rate in the following stationkeeping stage (see Fig. 12b). The results in Figs. 12c and 12d illustrate that the system configuration has just a small excursion from its initial lineal configuration, and the out-of-plane libration motions are closed within a stable range (± 6 deg relative to desired positions). Although the retrieval makes the orbit motion of the parent satellite less stable than in the stationkeeping case (see Fig. 12a), the spin rate increases as the tether length decreases, rendering the attitude motion more stable.

V. Conclusions

An extended HAS model of multitethered satellite formations permitting an additional degree of freedom to take into account a variable-length tether during the reconfiguration stage is proposed. Based on the HRTBP, a new formulation for the analysis of the three-dimensional nonlinear dynamics of a multitethered system near the second collinear libration point (L_2) is developed.

For the static formations in which the parent satellite is located very close to L_2, we draw a number of conclusions. During stationkeeping, as the tether lengths or mass ratios increase, the distance between the equilibrium position of the parent satellite and L_2 increases, and the motion of the parent satellite is less stable for larger initial equilibrium positions. However, the change of equilibrium position has almost no impact on in-plane or out-of-plane tether librations. The parent satellite will move slowly away from its initial position for both deployment and retrieval, and the excursions during retrieval are larger than those during deployment at the same relative time. The in-plane and out-of-plane tether librations during deployment are more stable than those during retrieval. Additionally, the deployment stage is more conducive to keeping the system in its initial configuration compared with the retrieval stage.

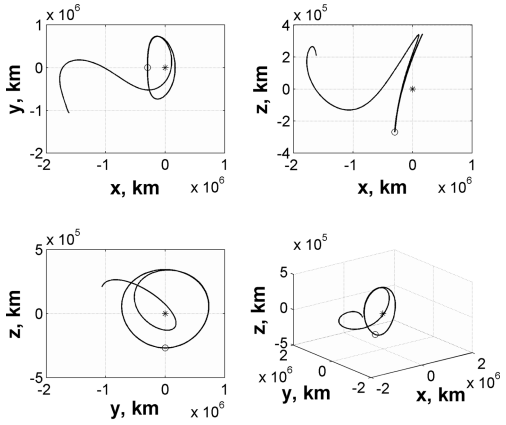

a) Halo orbit motion (4T)

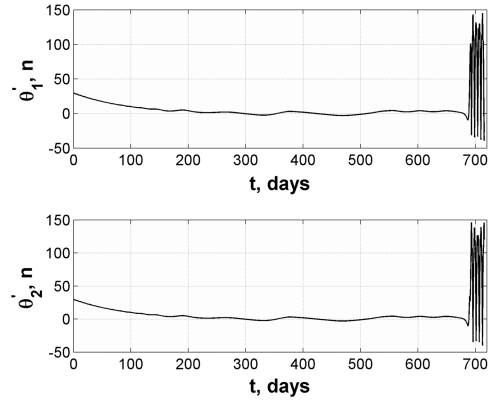

b) In-plane tether angular velocities

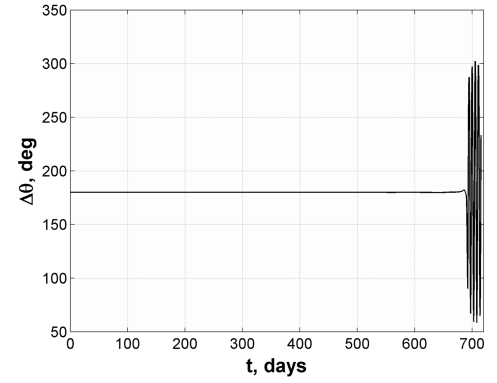

c) In-plane relative angle ($\Delta\theta = \theta_2 - \theta_1$)

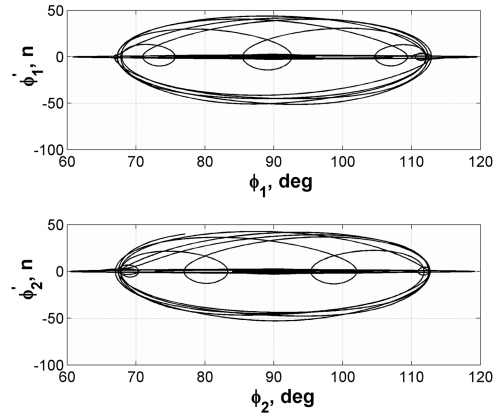

d) Phase portrait of out-of-plane tether librations

Fig. 11 Stability during deployment under the exponential tether law ($\lambda_e = 0.3$).

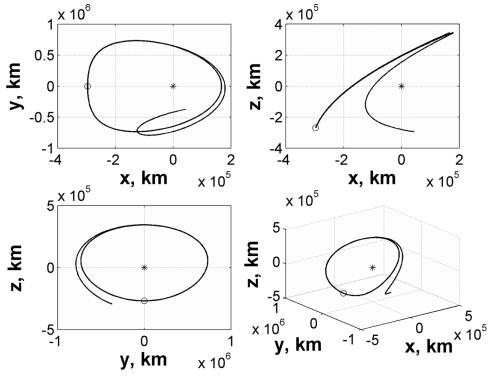

a) Halo orbit motion (4T)

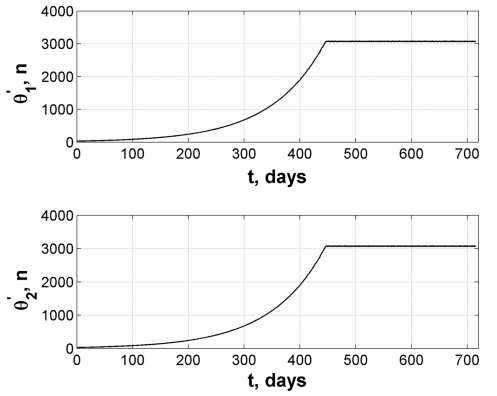

b) In-plane tether angular velocities

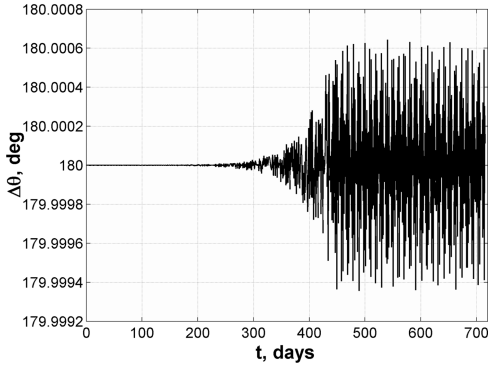

c) In-plane relative angle ($\Delta\theta = \theta 2 - \theta 1$)

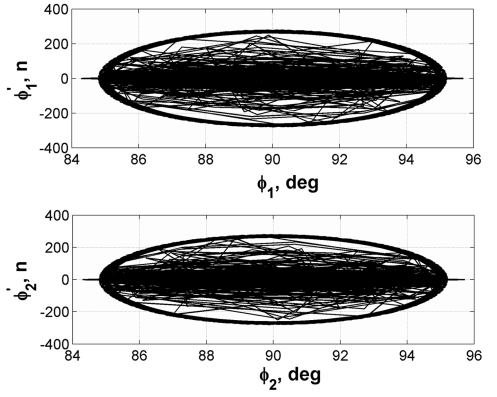

d) Phase portrait of out-of-plane tether librations

Fig. 12 Stability during retrieval under the exponential tether law ($\lambda_e = -0.3$).

For the dynamic formations in which the parent satellite is prescribed to larger periodic halo orbits, the coupling dynamics between the rotating tethers and the orbital motion are simulated during the stationkeeping stage. The results show that spin stabilizing for the multitethered satellite formation in a large halo orbit is dynamically possible. The range of out-of-plane librations increases with increasing orbit amplitudes of the parent satellite. The southern halo orbit provides a more stable planar configuration when compared with the northern halo orbit. The orbit and attitude motions of the tethered formation with a small mass ratio are more stable than those with a large mass ratio. Finally, the coupling dynamics of dynamic formations during the reconfiguration stage are investigated by assuming the tether length changes under an exponential tether law during both deployment and retrieval. During deployment, the in-plane angular velocities decrease to zero, and the out-of-plane librations depart far from their desired positions. The system will not maintain its desired initial lineal configuration. During retrieval, the in-plane angular velocities increase from their initial rate to a higher rate for the whole retrieval and then maintain this rate unchanged in the following stationkeeping stage. The system configuration undergoes minor excursions from its initial lineal configuration, and the out-of-plane libration motions are closed within a stable range. Although the retrieval makes the orbit motion of the parent satellite less stable than in the stationkeeping case, the spin rate increases as the tether lengths decrease; this can stabilize the attitude motion.

Although the accurate initial conditions are given, the parent satellite will depart from the desired halo orbit after several periods because of the inherent instabilities of libration point orbits and the perturbation of subsatellites. The attitude motions will be no more stable. The possibility of adding active control strategies for further improving the long-term stability and robustness characteristics of the tethered system will be explored in the future, for both orbit motion and tether librations simultaneously.

Appendix A: Terms in Eq. (12)

$$
\begin{aligned}
F_{xi} = \mu_i\{ & l_{di}[-\theta_i'' \sin\theta_i \sin\phi_i + \phi_i'' \cos\theta_i \cos\phi_i \\
& - 2\phi_i'(\theta_i' + 1)\sin\theta_i \cos\phi_i \\
& - (\phi_i'^2 + (\theta_i' + 1)^2 + 2)\cos\theta_i \sin\phi_i - f_{i1}] + g_{i1} \\
& + 2l_{di}'[-(\theta_i' + 1)\sin\theta_i \sin\phi_i \\
& + \phi_i' \cos\theta_i \cos\phi_i] + l_{di}'' \cos\theta_i \sin\phi_i\}
\end{aligned} \tag{A1}
$$

$$
\begin{aligned}
F_{yi} = \mu_i\{ & l_{di}[\theta_i'' \cos\theta_i \sin\phi_i + \phi_i'' \sin\theta_i \cos\phi_i \\
& + 2\phi_i'(\theta_i' + 1)\cos\theta_i \cos\phi_i \\
& - (\phi_i'^2 + (\theta_i' + 1)^2 - 1)\sin\theta_i \sin\phi_i - f_{i2}] \\
& + g_{i2} + 2l_{di}'[(\theta_i' + 1)\cos\theta_i \sin\phi_i \\
& + \phi_i' \sin\theta_i \cos\phi_i] + l_{di}'' \sin\theta_i \sin\phi_i\}
\end{aligned} \tag{A2}
$$

$$
\begin{aligned}
F_{zi} = \mu_i\{ & l_{di}[-\phi_i'' \sin\phi_i - (\phi_i'^2 - 1)\cos\phi_i - f_{i3}] + g_{i3} \\
& + 2l_{di}'\phi_i' \sin\phi_i + l_{di}'' \cos\phi_i\}
\end{aligned} \tag{A3}
$$

$$
\begin{aligned}
& f_{ij} = [u_{ij} - 3(\tilde{\boldsymbol{\rho}} \bullet \mathbf{u}_i)\tilde{\rho}_j]/r_p^3; \\
& g_{ij} = 3\varepsilon l_{di}^2[5(\tilde{\boldsymbol{\rho}} \bullet \mathbf{u}_i)^2\tilde{\rho}_j - 2(\tilde{\boldsymbol{\rho}} \bullet \mathbf{u}_i)u_{ij} - (\mathbf{u}_i \bullet \mathbf{u}_i)\tilde{\rho}_j]/(2r_p^4); \\
& j = 1, 2, 3
\end{aligned} \tag{A4}
$$

where $\tilde{\boldsymbol{\rho}} = [\,\tilde{\rho}_1 \quad \tilde{\rho}_2 \quad \tilde{\rho}_3\,]^T$, $\mathbf{u}_i = [\,u_{i1} \quad u_{i2} \quad u_{i3}\,]^T$, $\tilde{\rho}_1 = (1 + x)\varepsilon/r_P$, $\tilde{\rho}_2 = y\varepsilon/r_P$, $\tilde{\rho}_3 = z\varepsilon/r_P$, $u_{i1} = \cos\theta_i \sin\phi_i$, $u_{i2} = \sin\theta_i \sin\phi_i$, $u_{i3} = \cos\phi_i$

Appendix B: Terms in Eq. (13)

$$\lambda_{\theta_i} = \lambda_i \bullet \partial(\tilde{\boldsymbol{\rho}} \bullet \mathbf{u}_i)/\partial\theta_i \tag{B1}$$

$$\lambda_{\phi i} = \lambda_i \bullet \partial(\tilde{\boldsymbol{\rho}} \bullet \mathbf{u}_i)/\partial\phi_i \tag{B2}$$

$$\lambda_{l_{di}} = \lambda_i \bullet (\tilde{\boldsymbol{\rho}} \bullet \mathbf{u}_i)/l_{di} + (\mathbf{u}_i \bullet \mathbf{u}_i) l_{di}/r_p^3 \tag{B3}$$

where $\lambda_i = l_{di}/(\varepsilon r_p^2) - 3l_{di}^2(\tilde{\boldsymbol{\rho}} \bullet \mathbf{u}_i)/r_p^3$,

$$\partial(\tilde{\boldsymbol{\rho}} \bullet \mathbf{u}_i)/\partial\theta_i = -\tilde{\rho}_1 \sin\theta_i \sin\phi_i + \tilde{\rho}_2 \cos\theta_i \sin\phi_i$$

and

$$\partial(\tilde{\boldsymbol{\rho}} \bullet \mathbf{u}_i)/\partial\phi_i = \tilde{\rho}_1 \cos\theta_i \cos\phi_i + \tilde{\rho}_2 \sin\theta_i \cos\phi_i - \tilde{\rho}_3 \sin\phi_i$$

.

Acknowledgment

This work was supported by the National Natural Science Foundation of China (10972045).

References

[1] Farquhar, R. W., Dunham, D. W., Guo, Y. P., and McAdams, J. V., "Utilization of Libration Points for Human Exploration in the Sun–Earth–Moon System and Beyond," *Acta Astronautica*, Vol. 55, Nos. 3–9, Aug.–Nov. 2004, pp. 687–700. doi:10.1016/j.actaastro.2004.05.021

[2] Gomez, G., Lo, M., Masdemont, J., and Museth, K., "Simulation of Formation Flight Near Lagrange Points for the TPF Mission," *Advances in the Astronautical Sciences*, Vol. 109, No. 1, 2002, pp. 61–75.

[3] Johnson, L., Gilchrist, B., Estes, R. D., and Loremzini, E., "Overview of Future NASA Tether Applications," *Advances in Space Research*, Vol. 24, No. 8, 1999, pp. 1055–1063. doi:10.1016/S0273-1177(99)00553-0

[4] Misra, A. K., and Modi, V. J., "A Survey on the Dynamics and Control of Tethered Satellite Systems," *Advances in the Astronautical Sciences*, Vol. 62, 1987, pp. 667–719.

[5] Kumar, K. D., "Review of Dynamics and Control of Nonelectrodynamic Tethered Satellite Systems," *Journal of Spacecraft and Rockets*, Vol. 43, No. 4, July–Aug. 2006, pp. 705–720. doi:10.2514/1.5479

[6] Cartmell, M. P., and McKenzie, D. J., "A Review of Space Tether Research," *Progress in Aerospace Sciences*, Vol. 44, No. 1, Jan. 2008, pp. 1–21. doi:10.1016/j.paerosci.2007.08.002

[7] Misra, A. K., "Dynamics and Control of Tethered Satellite Systems," *Acta Astronautica*, Vol. 63, Nos. 11–12, 2008, pp. 1169–1177. doi:10.1016/j.actaastro.2008.06.020

[8] Williams, T., and Moore, K., "Dynamics of Tethered Satellite Formations," American Astronautical Society Paper 02-198, Jan. 2002.

[9] Cosmo, M. L., and Lorenzini, E. C., "Tethers in Space Handbook," 3rd ed., NASA, , 1997.

[10] Quinn, D. A., and Folta, D. C., "A Tether Formation Flying Concept for the SPECS Mission," American Astronautical Society Paper 01-404, Feb. 2001.

[11] Farley, R., and Quinn, D. A., "Tethered Formation Configurations: Meeting the Scientific Objectives of Large Aperture and Interferometric Science," 2001 AIAA GNC Conference, AIAA Paper 2001-4770, 2001.

[12] Kim, M., and Hall, C. D., "Dynamics and Control of Tethered Satellite Systems for NASA's SPECS Mission," American Astronautical Society Paper 03-532, Aug. 2003.

[13] Leisawitz, D., "NASA's Far-IR/Sub-Millimeter Roadmap Missions: SAFIR and SPECS," *Advances in Space Research*, Vol. 34, No. 3, 2004, pp. 631–636. doi:10.1016/j.asr.2003.06.023

[14] Decou, A. B., "Tether Static Shape for Rotating Multi-Mass, Multi-Tether, Spacecraft for 'Triangle' Michelson Interferometer," *Journal of Guidance, Control, and Dynamics*, Vol. 12, No. 2, March 1989, pp. 273–275. doi:10.2514/3.20401

[15] Misra, A. K., and Modi, V. J., "Three-Dimensional Dynamics and Control of Tethered Connected *N*-Body Systems," *Acta Astronautica*, Vol. 26, No. 2, 1992, pp. 77–84. doi:10.1016/0094-5765(92)90048-N

[16] Kumar, K. D., and Yasaka, T., "Rotating Formation Flying of Three Satellites Using Tethers," *Journal of Spacecraft and Rockets*, Vol. 41, No. 6, Nov.–Dec. 2004, pp. 973–985. doi:10.2514/1.14251

[17] Tragesser, S. G., and Tuncay, A., "Orbital Design of Earth-Oriented Tethered Satellite Formations," *Journal of the Astronautical Sciences*, Vol. 53, No. 1, Jan.–March 2005, pp. 51–64.

[18] Williams, P., "Optimal Deployment/Retrieval of a Tethered Formation Spinning in the Orbital Plane," *Journal of Spacecraft and Rockets*, Vol. 43, No. 3, May–June 2006, pp. 638–650. doi:10.2514/1.17093

[19] Gates, S. S., "Multi-Tethered Space-Based Interferometers: Particle System Model," Naval Research Laboratory, Rept. 20375-5320, Washington, DC, Sept. 2001.

[20] Farquhar, R. W., "Tether Stabilization at a Collinear Libration Point," *Journal of the Astronautical Sciences*, Vol. 49, No. 1, Jan.–March 2001, pp. 91–106.

[21] Misra, A. K., Bellerose, J., and Modi, V. J., "Dynamics of a Tethered System Near the Earth–Moon Lagrangian Points," *Advances in the Astronautical Sciences*, Vol. 109, No. 1, 2002, pp. 415–435.

[22] Peláez, J., Sanjurjo, R. M., Lucas, F. R., Lara, M., Lorenzini, E. C., Curreli, D., Scheeres, D. J., Bombardelli, C., and Dario, I., "Dynamics and Stability of Tethered Satellites at Lagrangian Points," ESA Rept. ACT/RPT/MAD/ART/07-4201, Nov. 2008.

[23] Wong, B., and Misra, A. K., "Dynamics of Lagrangian Point Multi-Tethered Satellite Systems," *Journal of the Astronautical Sciences*, Vol. 53, No. 3, July–Sept. 2005, pp. 221–250.

[24] Zhao, J., and Cai, Z. Q., "Nonlinear Dynamics and Simulation of Multi-Tethered Satellite Formations in Halo Orbits," *Acta Astronautica*, Vol. 63, Nos. 5–6, 2008, pp. 673–681. doi:10.1016/j.actaastro.2008.04.007

[25] Kim, M., and Hall, C. D., "Control of a Rotating Variable-Length Tethered System," *Journal of Guidance, Control, and Dynamics*, Vol. 27, No. 5, Sept.–Oct. 2004, pp. 849–858. doi:10.2514/1.3226

[26] Wong, B., and Misra, A. K., "Planar Dynamics of Variable Length Multi-Tethered Spacecraft near Collinear Lagrangian Points," *Acta Astronautica*, Vol. 63, Nos. 11–12, 2008, pp. 1178–1187. doi:10.1016/j.actaastro.2008.06.022

[27] Villac, B. F., "Dynamics in the Hill Problem with Applications to Spacecraft Maneuvers," Ph.D. Dissertation, Univ. of Michigan, Ann Arbor, MI, 2003.

[28] Scheeres, D. J., Hsiao, F. Y., and Vinh, N. X., "Stabilizing Motion Relative to an Unstable Orbit: Applications to Spacecraft Formation Flight," *Journal of Guidance, Control, and Dynamics*, Vol. 26, No. 1, 2003, pp. 62–73. doi:10.2514/2.5015

[29] Popescu, M., and Cardos, V., "The Domain of Initial Conditions for the Class of Three-Dimensional Halo Periodical Orbits," *Acta Astronautica*, Vol. 36, No. 4, Aug. 1995, pp. 193–196. doi:10.1016/0094-5765(95)00107-B

[30] Richardson, D. L., "Analytic Construction of Periodic Orbits About the Collinear Points," *Celestial Mechanics and Dynamical Astronomy*, Vol. 22, No. 3, Oct. 1980, pp. 241–253. doi:10.1007/BF01229511